19th International Conference
ENGINEERING MECHANICS 2013
Svratka, Czech Republic, May 13 – 16, 2013

Meshless local Petrov-Galerkin formulation for analysis of composite plates reinforced by unidirectional fibers

D. Riecky*, A. Sapietová, M. Žmindák****

Abstract: *This paper deals with application of the meshless methods for analysis of composite plates. The main focus is on the implementation of the MLPG formulation for layered plates. For this purpose the implementation of homogenization theory was required and analyses were performed in order to obtain homogenized material properties of composite plates. The software for homogenization of material properties uses direct homogenization method that is based on volume average of stresses in the representative volume element (RVE). Homogenization is performed by a multisoftware approach, by linking MATLAB and ANSYS software. Data obtained are used in analyses performed in own software, which is based on the MLPG method. Strain, stress and displacement fields were evaluated. Results obtained by MLPG were compared with those obtained by FEM programs ANSYS and ABAQUS.*

Keywords: ***Composite plates, unidirectional composites, Reissner-Mindlin theory, meshless method***

1. Introduction

Plate and shell structures are the most widely used structural members in mechanical and civil engineering thanks to their good weight to load carrying capability ratio. Pipes, aeroplanes, hulls of ships, bridge reinforcements as well as reinforced roofs and membranes are good examples.

Thanks to good material properties, especially to good weight to strength ratio fiber-reinforced materials came into practice. Laminates are composed of multiple layers where fiber orientation in particular layers can be different. By this way it is possible to obtain required material properties in required direction.

The finite element method (FEM) is one of the most widely used and most popular numerical methods for analyzing plate structures. Although the method is stable, well developed and has reached extensive development during last decades, it also has some limitations. One of the assumptions in FEM is an existence of the mesh created from the finite elements. Mesh quality affects the accuracy of solution and stability of convergence. Creating well defined meshes can be very time consuming in some cases. Generally it is recommended to use finite elements with shapes which are the most similar to ideal shapes. Degenerated geometry or deformed shape can have a negative effect on the solution accuracy. This is very important in analyzing nonlinear problems with large deflections or large strains such as metal forming, fragmentation after impact, etc. In these cases an improper mesh causes serious decrease of accuracy or failure of computation.

In last years an increase of interest in new type of numerical methods known as meshless methods was observed (Sladek, et al.,2002, Soares, et al., 2012) These methods are interesting due to their flexibility and ability of solving boundary value problems without predefined mesh. Computational model in these methods is represented by a set of nodes distributed within global domain and its boundary. These nodes do not have to be connected into explicitly defined elements. Information about relations between the nodes is theoretically not necessary before analysis. By this way some problems with the mesh as in FEM can be overpassed. Problems with remeshing can be overpassed by

* Ing. Daniel Riecky, PhD.: Plastic Omnium Auto Exteriorx, LtD. 900 55 Lozorno, Slovakia, e-mail: riecky@plasticomnium.com

** doc. Ing Alžbeta Sapietová, PhD., University of Žilina, Faculty of Mechanical Engineering, Department of Applied Mechanics, Univerzitná 1, 010 26 Žilina, Slovak Republic, e-mail:alzbeta.sapietova@fstroj.uniza.sk

** prof. Ing. Milan Žmindák, CSc.: University of Žilina, Faculty of Mechanical Engineering, Department of Applied Mechanics, Univerzitná 1, 010 26 Žilina, Slovak Republic, e-mail:milan.zmindak@fstroj.uniza.sk

adding or removing some nodes as necessary. In some methods the resultant stress fields are globally continuous and this simplifies consequent analyses.

One of the areas where meshless methods are convenient to use is analysis of plate and shell structures. These methods are useful due to flexibility of meshless algorithms and ability of meshless approximation functions to obtain interpolating field with high order of continuity in simple way. In some cases it is possible to overcome some "locking" effects in more simple way than in FEM. Meshless methods are relatively new concept in computational mechanics. Compared to FEM formulations there are less meshless formulations available for plate and shell structures. Additional research and development of general meshless methods able to successfully solve various problems in plate structural analyses is therefore necessary.

2. Homogenization of composite

2.1. Homogenization techniques

There are various homogenization methods. Direct homogenization is based on the volume average of field variables, such as stress, strain and energy density. Effective properties can be calculated from effective properties definitions. The mean and calculation of field variables can be performed numerically, for example by FEM, BEM and the geometry and microstructural properties can be generalized.

Indirect homogenization is based on the Eshelby solution of self-deformation for one inclusion in an infinite matrix – the equivalent inclusion method (Eshelby, 1957). This method does not use averaging of the field variables and the effective properties can be obtained by deducing from the volume fractions and the inclusion geometry as well as the component properties. According to this pattern these methods were developed: self-consistent scheme (Hill, 1965), generalized self-consistent scheme (Christensen & Lo, 1979), differential methods (Norris, 1985), Mori-Tanaka method (Mori and & Tanaka, 1973). They are often used to calculate various properties of composites. But the generalized microstructural morphology, which is often present in real materials, cannot be handled out deterministically in these models. Constitutive responses of the component phases are limited and the estimated results with large disagreements are not reliable enough. These models cannot catch the effects of local non-homogeneities due to insufficient representation of microscopic stresses and strains.

An alternate approach to direct and indirect homogenization is the variational method, which can determine the upper and lower limits of the elasticity modulus (Hashin & Shtrikman, 1962).

A relatively new approach a homogenization of microstructures consist of mathematical homogenization based on a two-scale extension of the displacement field. This comes from the analysis of physical systems containing two or more scales (Bensoussan et al., 1978). This approach is good for multiphase materials, in which the natural scales are the microscopic scales, characteristic heterogenity or local discontinuity spacing. Macroscopic scales are characterized by the body dimensions. This method can be called the mathematical homogenization.

2.1. Results of homogenization

This part describes the procedure of homogenization of material properties of composites using the method of representative volume element (RVE). For the analysis of the material properties an own software was programmed in MATLAB language and a part of the solution was carried out in ANSYS software. The RVE consists of volume elements and is then loaded by unit strains in various directions. The effective lamina properties are obtained from the volume means of stress values obtained by loading the RVE.

Homogenized lamina RVE consists of a fibers and epoxy matrix. The fibers are from three material types: carbon, glass, polyaramid. We assumed cylindrical fiber shapes and an ideal cohesion between the fiber and the matrix. Used carbon fibers have an industrial labeling T300 and M40J. The glass fiber label is EGlass and S2Glass. Polyaramide fibers have the label K49. Fiber material properties are listed in Tab.1. and the matrix properties ale listed in Tab. 2. (Wallenberger & Bingham, 2010)

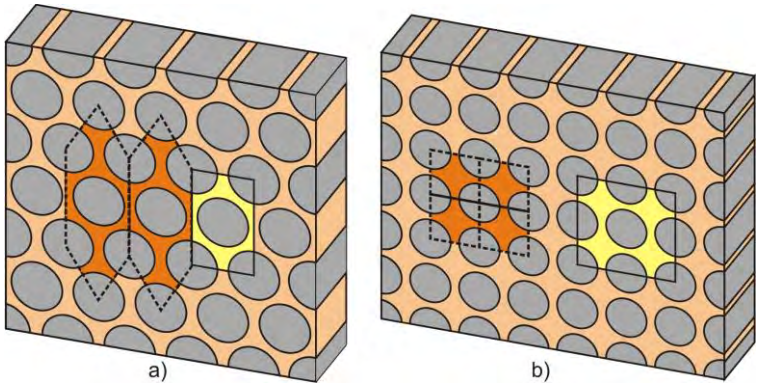

Fig. 1: Fiber arrangement in matrix a) hexagonal array b) square array

Tab. 1: Material properties of fibers

	Material of fiber				
	Carbon		Glass		Kevlar
	T300	M40J	EGlass	S2Glass	K49
Young's modulus E_f[GPa]	230	377	73	85,5	135.5
Tensile strength [GPa]	3.53	4.41	3.2	4.6	3.5
Poisson's ratio	0.33	0.33	0.22	0.22	0.37
Density ρ_f [kg/m^3]	1760	1770	2540	2490	1450
Fiber diameter d_f [μm]	7	5	8	10	10

Tab. 2: Material properties of matrix

Material	Young's modulus E_m [GPa]	Tensile strength [MPa]	Poisson's ratio	Density ρ_m [kg/m^3]	Shear elasticity modulus G_m [GPa]
Epoxy	3.45	70	0.3	85.5	1.33

Tab. 3: Material properties for composite with fiber volume fraction of $V_f = 0.6$.

V_f= 0.6	M40J		S2Glass		K49	
	h	s	h	s	h	s
E_1 [*GPa*]	227.58	227.58	52.683	52.687	82.683	82.685
E_2 [*GPa*]	12.831	16.71	11.607	14.334	12.121	15.301
G_{12} [*GPa*]	5.15	5.53	4.67	4.94	4.844	5.155
G_{23} [*GPa*]	4.737	6.967	4.3314	5.905	4.481	6.288
v_{12}	0.320	0.321	0.246	0.245	0.347	0.348
v_{23}	0.354	0.199	0.340	0.214	0.352	0.217

We note that indices "*h*" and "*s*" in Tab.3 denotes hexagonal array and square array, respectively

The RVE dimensions are calculated for the hexagonal fiber configuration (Fig. 1a), from the relations (1) and for a square configuration the RVE dimensions are in Fig. 1b, calculated from the relations in (2).

$$a_2 = \sqrt{\frac{1}{8}\frac{\pi d_f^2}{V_f\, tg(60^0)}},\ a_3 = a_2.tg(60^0),\ a_1 = 0{,}5.a_2 \tag{1}$$

$$a_2 = \sqrt{\frac{1}{4}\frac{d_f^2\pi}{V_f}},\ a_3 = a_2,\ a_1 = 0{,}5.a_2, \tag{2}$$

where a_1 is the x-direction, in this case the fiber direction, a_2 is the y direction, orthogonal to the fiber direction, a_3 in direction z, transverse perpendicular to the fiber direction.

The basic scheme of homogenization of composite plate is shown in the Fig. 2.

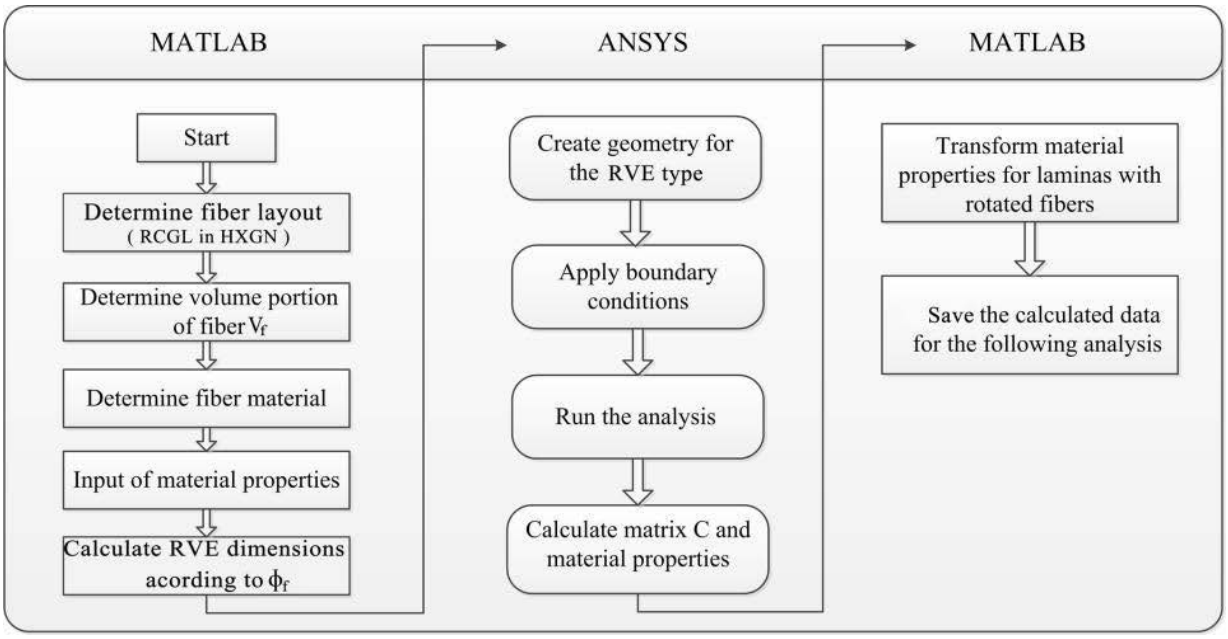

Fig. 2: Block scheme of the computation

3. Governing equations

Classical laminated plate theory was formulated by deriving classical plate theory for composite plates. In this theory the plate composes of N orthotropic layers with total thickness h. The midsurface of layered plate is located in the region Ω, in plane (x_1, x_2). Axis $x_3 \equiv z$ is perpendicular to the midsurface (Fig. 3). K-th layer is located between coordinates from $z = z_k$ to $z = z_{k+1}$ in thickness direction x_3.

Deformation of the plate is described by the "Reissner-Mindlin" plate theory (Reddy, 1997). In this theory the shear strains in thickness direction are constant and correction coefficients are necessary for calculation of transverse shear forces. Spatial displacement field caused by transverse loading can be expressed, in terms of (Reddy, 1997) for displacement components u_1, u_2, u_3 in the form of

$$\begin{aligned} u_1(\mathbf{x}, x_3, t) &= x_3 w_1(\mathbf{x}), \\ u_2(\mathbf{x}, x_3, t) &= x_3 w_2(\mathbf{x}), \\ u_3(\mathbf{x}, t) &= w_3(\mathbf{x}), \end{aligned} \tag{3}$$

where $\mathbf{x} = [x_1; x_2]^T$ is the position vector, $w_\alpha(x_1, x_2, t)$ are rotations about plane axes and $w_3(x_1; x_2, t)$ is deflection from (x_1, x_2) plane.

Linear strains are given by

$$
\begin{aligned}
\varepsilon_{11}(\mathbf{x},x_3,t) &= x_3 w_{1,1}(\mathbf{x}),\\
\varepsilon_{22}(\mathbf{x},x_3,t) &= x_3 w_{2,2}(\mathbf{x}),\\
\varepsilon_{12}(\mathbf{x},x_3,t) &= x_3\left[w_{1,2}(\mathbf{x}) + w_{2,1}(\mathbf{x})\right]/2,\\
\varepsilon_{13}(\mathbf{x},t) &= \left[w_1(\mathbf{x}) + w_{3,1}(\mathbf{x})\right]/2,\\
\varepsilon_{23}(\mathbf{x},t) &= \left[w_2(\mathbf{x}) + w_{3,2}(\mathbf{x})\right]/2,
\end{aligned}
\tag{4}
$$

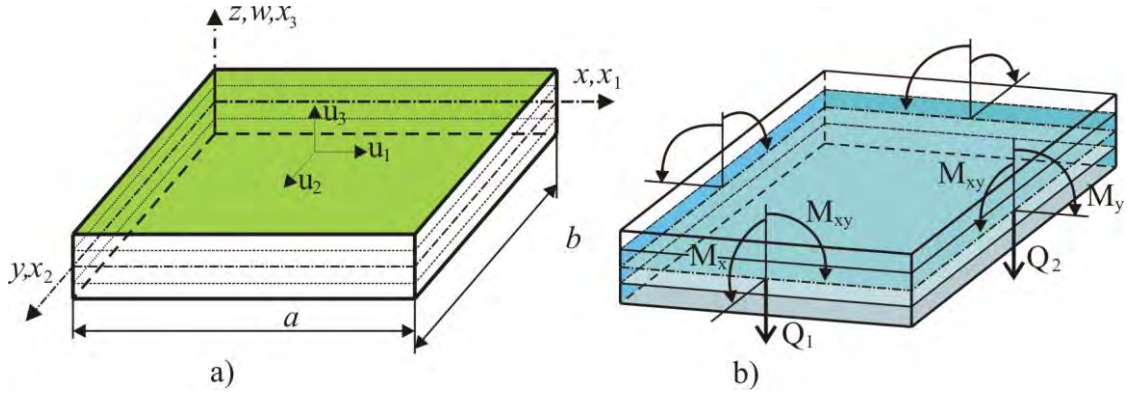

Fig. 3: Composite plate a) geometry and displacements, b) moments and shear forces

If k-th lamina is from orthotropic material, then the relation between stresses σ_{ij} and strains ε_{mn} is expressed by the constitutive equation for stress tensor

$$
\sigma_{ij}^{(k)}(\mathbf{x},x_3,t) = c_{ijmn}^{(k)}\varepsilon_{mn}(\mathbf{x},x_3,t),
\tag{5}
$$

with assumption of homogeneous coefficients of constitutive tensor $c_{ijmn}^{(k)}$ for k-th lamina.

From the equation (4) it can be seen that strains are continuous through the plate thickness. Discontinuous material coefficients cause the stiffness change in the interfaces and hence the stresses in lamina interfaces are discontinuous.
Equation (5) for plate problems is usually written as a tensor of elastic constants of the second order. Constitutive equations for orthotropic material and plane stress have then the form of

$$
\begin{bmatrix}\sigma_{11}\\ \sigma_{22}\\ \sigma_{12}\\ \sigma_{13}\\ \sigma_{23}\end{bmatrix} = \mathbf{G}^{(k)}(\mathbf{x})\begin{bmatrix}\varepsilon_{11}\\ \varepsilon_{22}\\ 2\varepsilon_{12}\\ 2\varepsilon_{13}\\ 2\varepsilon_{23}\end{bmatrix},
\tag{6}
$$

where

$$
\mathbf{G}^{(k)}(\mathbf{x}) = \begin{bmatrix}
E_1^{(k)}/e^{(k)} & E_1^{(k)}v_{21}^{(k)}/e^{(k)} & 0 & 0 & 0\\
E_2^{(k)}v_{12}^{(k)}/e^{(k)} & E_2^{(k)}/e^{(k)} & 0 & 0 & 0\\
0 & 0 & G_{12}^{(k)} & 0 & 0\\
0 & 0 & 0 & G_{13}^{(k)} & 0\\
0 & 0 & 0 & 0 & G_{23}^{(k)}
\end{bmatrix}
$$

where $e^{(k)} = 1 - v_{12}^{(k)}v_{21}^{(k)}$, $E_\alpha^{(k)}$ is Young's elasticity modulus in x_α (α = 1, 2) -axis direction, $G_{12}^{(k)}$, $G_{13}^{(k)}$ and $G_{23}^{(k)}$ are shear elasticity moduli and $v_{\alpha\beta}^{(k)}$ are Poisson's ratios of k-th lamina.

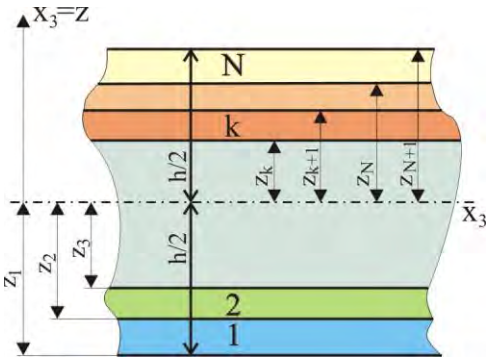

Fig. 4: Notations for a multilayered plate

Bending moments $M_{\alpha\beta}$ and Q_α can be expressed in integral form as

$$\begin{bmatrix} M_{11} \\ M_{22} \\ M_{12} \end{bmatrix} = \int_{-h/2}^{h/2} \begin{bmatrix} \sigma_{11} \\ \sigma_{22} \\ \sigma_{12} \end{bmatrix} x_3 dx_3 = \sum_{k=1}^{N} \int_{z_k}^{z_{k+1}} \begin{bmatrix} \sigma_{11} \\ \sigma_{22} \\ \sigma_{12} \end{bmatrix}^{(k)} x_3 dx_3 \tag{7}$$

$$\begin{bmatrix} Q_1 \\ Q_2 \end{bmatrix} = \kappa \int_{-h/2}^{h/2} \begin{bmatrix} \sigma_{13} \\ \sigma_{23} \end{bmatrix} dx_3 = \kappa \sum_{k=1}^{N} \int_{z_k}^{z_{k+1}} \begin{bmatrix} \sigma_{13} \\ \sigma_{23} \end{bmatrix}^{(k)} dx_3, \tag{8}$$

where $\kappa = 5/6$ in the Reisner-Mindlin plate theory, z coordinate is considered as is shown in Fig. 3. By substituting (6) and (4) into resultant moments and forces in (7), (8) it is possible to express bending moments $M_{\alpha\beta}$ and shear forces Q_α, α, β=1,2 for orthotropic plate in terms of displacements and rotations. In the case of layer-wise continuous material properties the following relations are obtained

$$\begin{aligned} M_{\alpha\beta} &= D_{\alpha\beta}(w_{\alpha,\beta} + w_{\beta,\alpha}) + C_{\alpha\beta} w_{\gamma,\gamma} \\ Q_\alpha &= C_\alpha (w_\alpha + w_{3,\alpha}). \end{aligned} \tag{9}$$

For repeated indices α and β in (9) Einstein summation rule does not apply and material parameters $D_{\alpha\beta}$ and $C_{\alpha\beta}$ are given by relations

$$\begin{aligned} 2D_{11} &= \int_{-h/2}^{h/2} z^2 E_1(z) \frac{1-\nu_{21}}{e} dz = \sum_{k=1}^{N} \int_{z_k}^{z_{k+1}} E_1^{(k)} \frac{1-\nu_{21}^{(k)}}{e^{(k)}} z^2 dz = \sum_{k=1}^{N} E_1^{(k)} \frac{1-\nu_{21}^{(k)}}{e^{(k)}} \frac{1}{3}\left(z_{k+1}^3 - z_k^3\right), \\ 2D_{22} &= \int_{-h/2}^{h/2} z^2 E_2(z) \frac{1-\nu_{12}}{e} dz = \sum_{k=1}^{N} E_2^{(k)} \frac{1-\nu_{12}^{(k)}}{e^{(k)}} \frac{1}{3}\left(z_{k+1}^3 - z_k^3\right), \\ D_{12} &= \int_{-h/2}^{h/2} z^2 G_{12}(z) dz = \sum_{k=1}^{N} G_{12}^{(k)} \frac{1}{3}\left(z_{k+1}^3 - z_k^3\right), \\ C_{11} &= \int_{-h/2}^{h/2} z^2 E_1(z) \frac{\nu_{21}}{e} dz = \sum_{k=1}^{N} E_1^{(k)} \frac{\nu_{21}^{(k)}}{e^{(k)}} \frac{1}{3}\left(z_{k+1}^3 - z_k^3\right), \\ C_{22} &= \int_{-h/2}^{h/2} z^2 E_2(z) \frac{\nu_{12}}{e} dz = \sum_{k=1}^{N} E_1^{(k)} \frac{\nu_{21}^{(k)}}{e^{(k)}} \frac{1}{3}\left(z_{k+1}^3 - z_k^3\right), \\ C_{12} &= C_{21} = 0, \\ C_\alpha &= \kappa \int_{-h/2}^{h/2} G_{\alpha 3}(z) dz = \kappa \sum_{k=1}^{N} G_{\alpha 3}\left(z_{k+1}^3 - z_k^3\right). \end{aligned} \tag{10}$$

For homogeneous plate relations (10) are simplified to the form of

$$D_{11} = \frac{D_1}{2}\left(1-\nu_{21}\right), \quad D_{22} = \frac{D_2}{2}\left(1-\nu_{12}\right), \quad D_{12} = D_{21} = \frac{G_{12} h^3}{12},$$

$$C_{11} = D_1 v_{21},\ C_{22} = D_2 v_{12},\ \ C_{12} = C_{21} = 0,$$

$$D_\alpha = \frac{E_\alpha h^3}{12e},\ \ D_1 v_{21} = D_2 v_{12},\ \ C_\alpha = \kappa h G_{\alpha 3}. \tag{11}$$

Plate is subjected to transverse distributed loading q(x, t). If each lamina has homogeneous density in thickness direction, equations of motion for Reissner linear theory for thick plates can be written in the form of

$$M_{\alpha\beta,\beta}(\mathbf{x},t) - Q_\alpha(\mathbf{x},t) = I_M \ddot{w}_\alpha(\mathbf{x},t), \tag{12}$$

$$Q_{\alpha,\alpha}(\mathbf{x},t) + q(\mathbf{x},t) = I_Q \ddot{w}_\alpha(\mathbf{x},t), \tag{13}$$

where the dot over a quantity indicates differentiations with respect to time t and indices α, β = 1, 2 and

$$\begin{aligned} I_M &= \int_{-h/2}^{h/2} z^2 \rho(z) dz = \sum_{k=1}^{N} \int_{z_k}^{z_{k+1}} \rho^{(k)} z^2 dz = \sum_{k=1}^{N} \rho_1^{(k)} \frac{1}{3}\left(z_{k+1}^3 - z_k^3\right), \\ I_Q &= \int_{-h/2}^{h/2} \rho(z) dz = \sum_{k=1}^{N} \int_{z_k}^{z_{k+1}} \rho^{(k)} dz = \sum_{k=1}^{N} \rho^{(k)} \left(z_{k+1}^3 - z_k^3\right), \end{aligned} \tag{14}$$

are global inertial characteristics of the laminated plate For constant mass density throughout the plate thickness, we obtain $I_M = \rho h^3 / 12$, $I_Q = \rho h$.

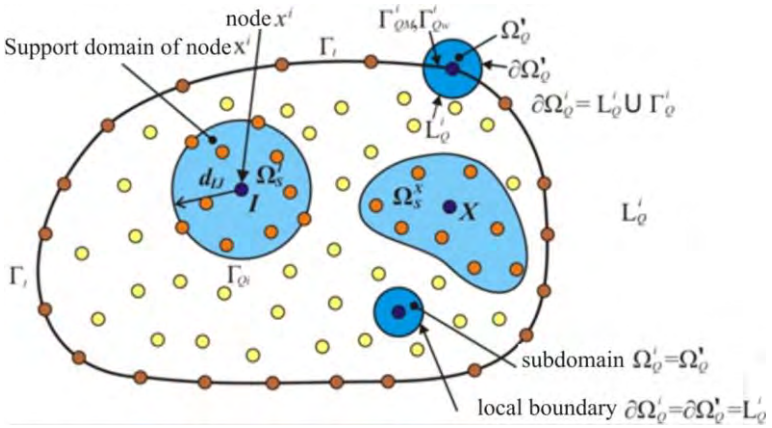

Fig. 5: Local boundaries for weak formulation, the support domain Ω_s for MLS approximation of the trial function, and support domain of weight function around node x^i, Ω_Q is integration domain around given node.

In MLPG method the local weak form is assembled on local subdomain Ω_Q, which is a small domain for each node within the global domain (Atluri, 2004). These local subdomains overlap each other and cover the whole global domain Ω, Fig. 13. Local weak form of the governing equations (12) and (13) for $x^i \in \Omega^i_Q x^i$ can have the form of

$$\int_{\Omega^i_Q} \left[M_{\alpha\beta,\beta}(\mathbf{x},t) - Q_\alpha(\mathbf{x},t) - I_M \ddot{w}_\alpha(\mathbf{x},t)\right] w^*_{\alpha\gamma}(\mathbf{x}) d\Omega = 0, \tag{15}$$

$$\int_{\Omega^i_Q} \left[Q_{\alpha,\alpha}(\mathbf{x},t) - q(\mathbf{x},t) - I_Q \ddot{w}_3(\mathbf{x},t)\right] w^*(\mathbf{x}) d\Omega = 0, \tag{16}$$

where $w^*_{\alpha\gamma}$ and w^* are weight and testing function, respectively. Applying the Gauss divergence theorem to Eqs. (15) and (16) one obtains

$$\int_{\partial\Omega_Q^i} M_\alpha(\mathbf{x},t)w^*_{\alpha\gamma}(\mathbf{x})d\Gamma - \int_{\Omega_Q^i} M_{\alpha\beta}(\mathbf{x},t)w^*_{\alpha\gamma,\beta}(\mathbf{x})d\Omega - \int_{\Omega_Q^i} Q_\alpha(\mathbf{x},t)w^*_{\alpha\gamma}(\mathbf{x})d\Omega - \\ - \int_{\Omega_Q^i} I_M \ddot{w}^*_{\alpha\gamma}(\mathbf{x},t)w^*_{\alpha\gamma}(\mathbf{x})d\Omega = 0, \tag{17}$$

$$\int_{\partial\Omega_Q^i} Q_\alpha(\mathbf{x})n_\alpha(\mathbf{x})w^*(\mathbf{x})d\Gamma - \int_{\Omega_Q^i} Q_\alpha(\mathbf{x})w^*_{,\alpha}(\mathbf{x})d\Omega - \int_{\Omega_Q^i} I_Q \ddot{w}^*_3(\mathbf{x},t)w^*(\mathbf{x})d\Omega + \\ + \int_{\Omega_Q^i} q(\mathbf{x})w^*(\mathbf{x})d\Omega = 0, \tag{18}$$

where $\partial\Omega_Q^i$ is boundary of local subdomain, $M_\alpha(\mathbf{x}) = M_{\alpha\beta}(\mathbf{x})n_\beta(\mathbf{x})$ is the normal bending moment and n_α is the outward normal on the boundary $\partial\Omega_Q^i$. Local weak forms (17) and (18) are starting points for deriving local boundary integral equations on the basis of proper test function. Unit step function is chosen in each subdomain for test functions $w^*_{\alpha\gamma}(\mathbf{x})$ and $w^*(\mathbf{x})$

$$w^*_{\alpha\gamma}(\mathbf{x}) = \begin{cases} \delta_{\alpha\gamma} & \text{v} \quad \mathbf{x} \in (\Omega \cup \partial\Omega_s) \\ 0 & \text{v} \quad \mathbf{x} \notin (\Omega \cup \partial\Omega_s) \end{cases}, \quad w^*(\mathbf{x}) = \begin{cases} 1 & \text{v} \quad \mathbf{x} \in (\Omega \cup \partial\Omega_s) \\ 0 & \text{v} \quad \mathbf{x} \notin (\Omega \cup \partial\Omega_s) \end{cases} \tag{19}$$

Then the local weak form (15) and (16) transforms on the following local integral equations

$$\int_{\partial\Omega_Q^i} M_\alpha(\mathbf{x})d\Gamma - \int_{\Omega_Q^i} Q_\alpha(\mathbf{x})d\Omega - \int_{\Omega_Q^i} I_M \ddot{w}_\alpha(\mathbf{x})d\Omega = 0, \tag{20}$$

$$\int_{\partial\Omega_Q^i} Q_\alpha(\mathbf{x})n_\alpha(\mathbf{x})d\Gamma - \int_{\Omega_Q^i} I_Q \ddot{w}_3(\mathbf{x})d\Omega + \int_{\Omega_Q^i} q(\mathbf{x})d\Omega = 0, \tag{21}$$

where $w_\alpha(\mathbf{x};\, t)$ is the trial function corresponding to rotations , α = 1, 2, the trial function $w_3(\mathbf{x};\, t)$ corresponds to the transverse displacement. These trial functions are assembled in MLS approximation over nodes in local subdomain around the point x.

4. Numerical implementation MLPG for composite plate

In general, a meshless method uses a local interpolation to represent the trial function with the values (or the fictitious values) of the unknown variable at some randomly located nodes (Sladek et al., 2005). To approximate the distribution of the generalized displacements (rotations and deflection) in Ω_x over a number of randomly located nodes $\{\mathbf{x}^a\}$, a = 1, 2, ... n, the MLS approximant $w_i^h(\mathbf{x},t)$ of $w_i(\mathbf{x},t)$ is defined by

$$\mathbf{w}^h(\mathbf{x},t) = \sum_{a=1}^{n} \phi^a(\mathbf{x})\hat{\mathbf{w}}^a(t), \tag{22}$$

where $\mathbf{w}^h = [\, w_1^h, w_2^h, w_3^h \,]^T$, ϕ^a is shape function of MLS approximation corresponding to node $\boldsymbol{x}^a$. The directional derivatives of **w**(x,t) are approximated in terms of the same nodal values

$$\mathbf{w}_{,k}(\mathbf{x},t) = \sum_{a=1}^{n} \hat{\mathbf{w}}^a(t)\phi^a_{,k}(\mathbf{x}), \tag{23}$$

where $\phi^a_{,k}(\mathbf{x})$ is partial derivative of shape function $\phi^a(\mathbf{x})$ according to direction $k = x_1, x_2$.

Substituting the approximation (23) into the definition of the bending moments (9) and then using $M_\alpha(\mathbf{x};\, t) = M_{\alpha\beta}(\boldsymbol{x};\, t)\, \mathbf{n}_\beta(\boldsymbol{x})$, one obtains

$$\mathbf{M}(\mathbf{x}) = \mathbf{N}_1 \sum_{a=1}^{N} \mathbf{B}_1^a(\mathbf{x})\mathbf{w}^{*a} + \mathbf{N}_2 \sum_{a=1}^{N} \mathbf{B}_2^a(\mathbf{x})\mathbf{w}^{*a} = \mathbf{N}_\alpha(\mathbf{x}) \sum_{a=1}^{N} \mathbf{B}_\alpha^a(\mathbf{x})\mathbf{w}^{*a} \tag{24}$$

where vector $\mathbf{w}^{*a} = [\, \hat{w}_1^{*a}; \hat{w}_2^{*a} \,]^T$, the matrices $\mathbf{N}_\alpha(\mathbf{x})$ are related to the normal vector $\mathbf{n}(\mathbf{x})$ on $\partial\Omega_s$ by

$$\mathbf{N}_1(\mathbf{x})=\begin{bmatrix} n_1 & 0 & n_2 \\ 0 & n_2 & n_1 \end{bmatrix} \text{ a } \mathbf{N}_2(\mathbf{x})=\begin{bmatrix} C_{11} & 0 \\ 0 & C_{22} \end{bmatrix}\begin{bmatrix} n_1 & n_1 \\ n_2 & n_2 \end{bmatrix} \tag{25}$$

and the matrices $\mathbf{B}_\alpha^a$ are represented by the gradients of the shape functions as

$$\mathbf{B}_1^a(\mathbf{x})=\begin{bmatrix} 2D_{11}^a\phi_{,1}^a & 0 \\ 0 & 2D_{22}^a\phi_{,2}^a \\ D_{12}^a\phi_{,2}^a & D_{12}^a\phi_{,1}^a \end{bmatrix} \text{ and } \mathbf{B}_2^a(\mathbf{x})=\begin{bmatrix} \phi_{,1}^a & 0 \\ 0 & \phi_{,2}^a \end{bmatrix} \tag{26}$$

The influence of the material properties for composite laminates is incorporated into $C_{\alpha\beta}$ and $D_{\alpha\beta}$, defined in equations (10). Similarly one can obtain the approximation for the shear forces

$$\mathbf{Q}(\mathbf{x})=\mathbf{C}(\mathbf{x})\sum_{a=1}^{N}\left[\phi^a(\mathbf{x})\mathbf{w}^{*a}+\mathbf{F}^a(\mathbf{x})\hat{w}_3^{*a}\right] \tag{27}$$

where $\mathbf{Q}(\mathrm{x}) = [Q_1(\mathrm{x}) ; Q_2(\mathrm{x})]^T$ and

$$\mathbf{C}(\mathbf{x})=\begin{bmatrix} C_1(\mathbf{x}) & 0 \\ 0 & C_2(\mathbf{x}) \end{bmatrix},\ \mathbf{F}^a(\mathbf{x})=\begin{bmatrix} \phi_{,1}^a \\ \phi_{,2}^a \end{bmatrix} \tag{28}$$

Then, insertion of the MLS-discretized moment and force fields (26) and (29) into the local integral equations (17) and (18) yields the discretized local integral equations

$$\begin{aligned} &\sum_{a=1}^{n}\left[\int_{L_Q^i+\Gamma_{QM}^i}\mathbf{N}_\alpha(\mathbf{x})\mathbf{B}_\alpha^a(\mathbf{x})d\Gamma-\int_{\Omega_Q^i}\mathbf{C}(\mathbf{x})\phi^a(\mathbf{x})d\Omega\right]\mathbf{w}^{*a}- \\ &-\sum_{a=1}^{n}I_M\ddot{\mathbf{w}}^{*a}(t)\left(\int_{\Omega_Q^i}\phi^a(\mathbf{x})d\Omega\right)- \\ &-\sum_{a=1}^{n}\hat{w}_3^a\left[\int_{\Omega_Q^i}\mathbf{C}(\mathbf{x})\mathbf{F}^a(\mathbf{x})d\Omega\right]=-\int_{\Gamma_{QM}^i}\tilde{\mathbf{M}}(\mathbf{x})d\Gamma, \end{aligned} \tag{29}$$

$$\begin{aligned} &\sum_{a=1}^{n}\left[\int_{\partial\Omega_Q^i}\mathbf{C}_n(\mathbf{x})\phi^a(\mathbf{x})d\Gamma\right]\mathbf{w}^{*a}-\sum_{a=1}^{n}\hat{w}_3^a\left[\int_{\Omega_Q^i}\mathbf{C}_n(\mathbf{x})\mathbf{F}^a(\mathbf{x})d\Gamma\right]- \\ &-I_Q\sum_{a=1}^{n}\ddot{\hat{\mathbf{w}}}_3^a(t)\left(\int_{\Omega_Q^i}\phi^a(\mathbf{x})d\Omega\right)=-\int_{\Omega_Q^i}q(\mathbf{x})d\Omega, \end{aligned} \tag{30}$$

where $\tilde{\mathbf{M}}(\mathbf{x})$ represent the prescribed bending moments on Γ_{QM}^i and

$$\mathbf{C}(\mathbf{x})=(n_1,n_2)\begin{pmatrix} C_1 & 0 \\ 0 & C_2 \end{pmatrix}=(C_1n_1,C_2n_2) \tag{31}$$

Equations (29) and (30) are considered on the subdomains adjacent to the interior nodes $\mathbf{x}^i$ as well as to the boundary nodes on Γ_{QM}^i .

For the source point x^i located on the global boundary Γ the boundary of the subdomain $\partial\Omega_Q^i$ is decomposed into into L_Q^i a Γ_{QM}^i (part of the global boundary with prescribed bending moment), Fig. 5. It should be noted here that there are neither Lagrange multipliers nor penalty parameters introduced into the local weak-forms Γ_{QM}^i (part of the global boundary with prescribed rotations or displacements can be imposed directly, using the interpolation approximation (24)

$$\sum_{a=1}^{N}\phi^a(\mathbf{x}^i)\hat{\mathbf{w}}^a=\tilde{\mathbf{w}}(\mathbf{x}^i)\ \text{pre}\ (\mathbf{x}^i)\in\Gamma_{QM}^i, \tag{32}$$

where $\tilde{\mathbf{w}}(\mathbf{x}^i)$ is the generalized displacement vector prescribed on the boundary Γ_{QM}^i. For static loads following terms are zero

$$\sum_{a=1}^{n} I_M \ddot{\hat{\mathbf{w}}}_3^a(t) \left(\int_{\Omega_Q^i} \phi^a(\mathbf{x}) d\Omega \right) = 0 \tag{33}$$

$$-I_Q \sum_{a=1}^{n} \ddot{\hat{\mathbf{w}}}_3^a(t) \left(\int_{\Omega_Q^i} \phi^a(\mathbf{x}) d\Omega \right) = 0 . \tag{34}$$

Then, insertion of the MLS discretized moment and force fields into local integral equations into (29) and (30) we get the discretized local integral equations in the form

$$\sum_{a=1}^{n} \left[\int_{L_Q^i + \Gamma_{QM}^i} \mathbf{N}_\alpha(\mathbf{x}) \mathbf{B}_\alpha^a(\mathbf{x}) d\Gamma - \int_{\Omega_Q^i} \mathbf{C}(\mathbf{x}) \boldsymbol{\phi}^a(\mathbf{x}) d\Omega \right] \mathbf{w}^{*a} - \sum_{a=1}^{n} \hat{w}_3^a \left[\int_{\Omega_Q^i} \mathbf{C}(\mathbf{x}) \mathbf{F}^a(\mathbf{x}) d\Omega \right] = - \int_{\Gamma_{QM}^i} \tilde{\mathbf{M}}(\mathbf{x}) d\Gamma, \tag{35}$$

$$\sum_{a=1}^{n} \left[\int_{\partial\Omega_Q^i} \mathbf{C}_n(\mathbf{x}) \boldsymbol{\phi}^a(\mathbf{x}) d\Gamma \right] \mathbf{w}^{*a} - \sum_{a=1}^{n} \hat{w}_3^a \left[\int_{\Omega_Q^i} \mathbf{C}_n(\mathbf{x}) \mathbf{F}^a(\mathbf{x}) d\Gamma \right] = - \int_{\Omega_Q^i} q(\mathbf{x}) d\Omega, \tag{36}$$

Collecting the discretized local boundary-domain integral equations together with the discretized boundary conditions for the generalized displacements, one obtains a complete system of algebraic equations for calculation strain, stress and displacement fields.

5. Numerical example

In this section, numerical results are presented for laminated plates under a mechanical load. In order to test the accuracy, the numerical results obtained by the presented method are compared with the results provided by the FEM softwares ANSYS and ABAQUS.

Results obtained from own software were compared with reference values, which are in essence the mean values from values obtained from ANSYS and ABAQUS. The averaged percentage error was calculated from the following equation

$$APE = 100 \sqrt{\sum_{a=1}^{N} \left[\left(u^{ref}(x^a) - u^{MLPG}(x^a) \right)^2 \right] / \sum_{a=1}^{N} \left[\left(u^{ref}(x^a) \right)^2 \right]} \tag{35}$$

where N is total number of nodes in given domain, $u^{ref}(x^a)$ is the reference value in node x^a, $u^{MLPG}(x^a)$ is value calculated by means of MLPG in node x^a.

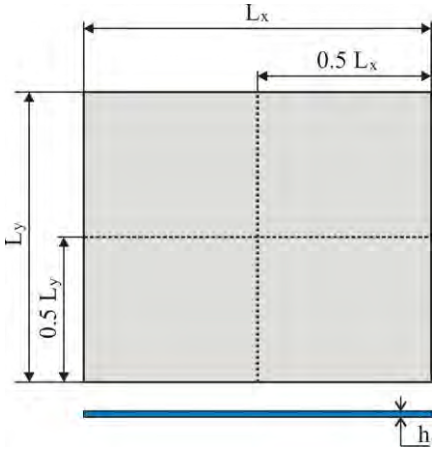

Fig. 6: Dimensions of plate and location of points for compare of results

Clamped and simply supported square plates are analysed. We consider composite plates with the dimensions L_x = 0.24 *m* and L_y = 0.2 *m*, Fig. 6. Is composed from six lamina with thickness Δ_z = 0.00025 *m*, total thickness of plate is h = 0.0015 *m*.

Material of the analyzed plate is EGlass_vf06. Maximum deflection of the plate is $w_{3\max}^{CC,MLPG} = \text{-}2.463\text{e-}3\,m$, the reference value is $w_{3\max}^{CC,ref} = \text{-}2.453\text{e-}3\,m$. Error in the point of maximum deflection is $\left|err_{w3}^{CC}\right| = 0.41\%$. The averaged percentage error is $ape_{w3}^{CC} = 2.37\%$ for computed deflections

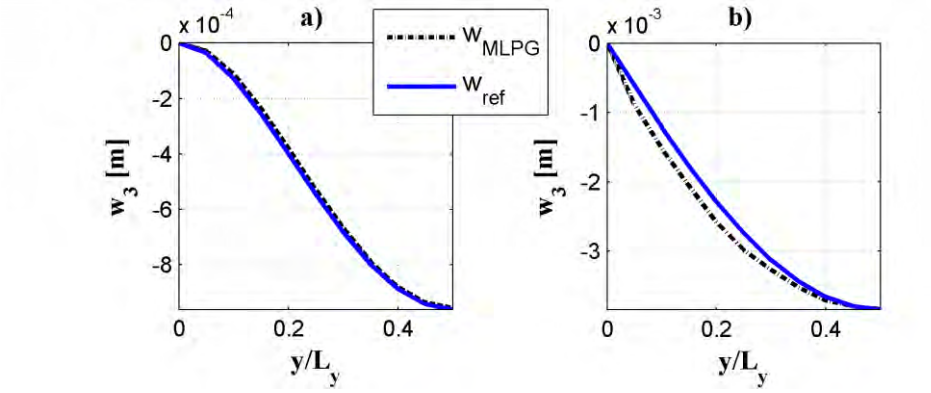

Fig 7: Comparison of deflection a)clamed plate, b) simply supported plate

Maximum deflection for simply supported plate is $w_{3\max}^{SS,MLPG} = \text{-}8.272\text{e-}3\,m$, the reference value for this degree of freedom is $w_{3\max}^{SS,ref} = 8.241\text{e-}3\,m$. Error in the point of maximum deflection is $\left|err_{w3}^{SSup}\right| = 0.38\%$. The averaged percentage error is $ape_{w3}^{SSup} = 2.25\%$. Deflections in Fig.7 is shown for $y = 0.5L_y$, Fig. 6.

The average percentage error in particular analyses is affected mainly by differences near the plate boundaries since these values are very small. And low reference values cause higher percentage errors as in points near the center of the plate. In the direction of the center of the plate the percentage differences with regard to the reference values decrease.

In this part course of deflections, strains and stresses in through the thickness direction are illustrated and values of these variables are listed in tables. Values are compared with reference results from FEM analyses. In each table absolute values of percentage differences with regard to the reference values are also listed. Plate dimensions are 0.24 x 0.2 *m*.

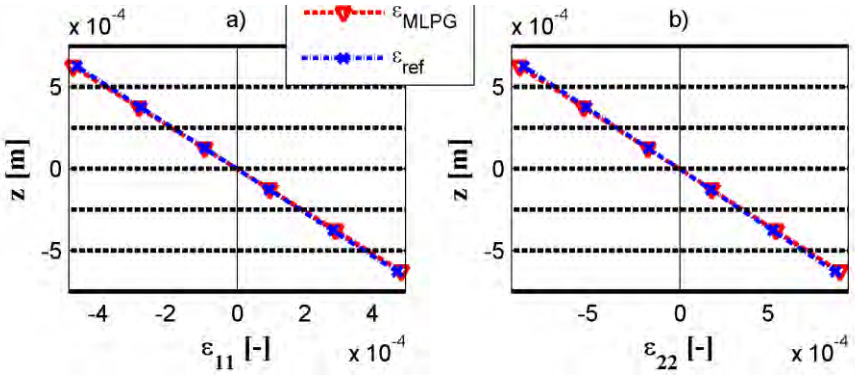

Fig. 8 : Course of strains through the thickness of plate from Glass_vf04, a) strain ε_{11}, b) strain ε_{22}

In Fig. 8 is described course of deformations ε_{11} and ε_{22} at point of maximum deflection of plate from material EGlass_vf04 and comparison of results are given in Tab. 4. In Fig. 9 is described course of stresses σ_{11} a σ_{22} at given point of plate from center of corresponding layer and values are given in Tab. 5.

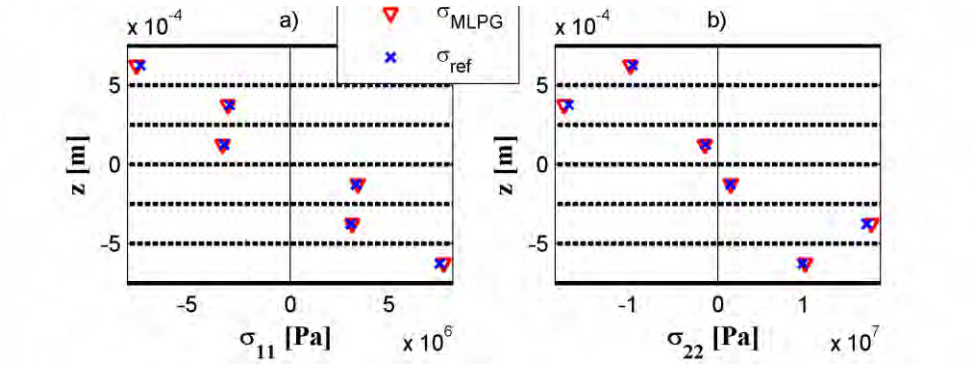

Fig. 9: The computed stress values at the center of layers EGlass_vf04, a) σ_{11}, b) σ_{22}

Tab. 4: Comparison of deformations ε_{11} a ε_{22} from MLPG and FEM, EGlass_vf04

layer	1	2	3	4	5	6
ε_1^{MLPG} [-]	4.85e-4	2.90e-4	0.969e-4	-0.969e-4	-2.90e-4	-4.85e-4
ε_1^{REF} [-]	4.74e-4	2.84e-4	0.948e-4	-0.948e-4	-2.84e-4	-4.74e-4
|err| [%]	2.3	2.3	2.3	2.3	2.3	2.3
ε_{22}^{MLPG} [-]	9.10e-4	5.46e-4	1.82e-4	-1.82e-4	-5.46e-4	-9.10e-4
ε_{22}^{REF} [-]	8.84e-4	5.31e-4	1.77e-4	-1.77e-4	5.31e-4	-8.84e-4
|err| [%]	2.95	2.95	2.95	2.95	2.95	2.95

Tab. 5: Comparison of stresses σ_{11} a σ_{22} from MLPG and FEM, Eglass_vf04

layer	1	2	3	4	5	6
σ_1^{MLPG} [-]	7.76e+6	3.14e+6	3.43e+6	-3.43e+6	-3.14e+6	-7.76e+6
σ_1^{REF} [-]	7.57e+6	3.07e+6	3.35e+6	-3.35e+6	-3.07e+6	-7.57e+6
|err| [%]	2.58	2.52	2.37	2.37	2.52	2.58
σ_{22}^{MLPG} [-]	10.20e+6	17.91e+6	1.50e+6	-1.50e+6	17.91e+6	-10.20e+6
σ_{22}^{REF} [-]	9.92e+6	17.4e+6	1.46e+6	-1.46e+6	-17.4e+6	-9.92e6
|err| [%]	2.85	2.94	2.88	2.88	2.94	2.85

6. Conclusions

The MLPG method was applied to analysis of laminated composite plates under static loadings. The numerical results confirm the fact that MLPG method is a good tool for analysis of composite structures. It is a reliable method after sufficient setting of parameters such as order of numerical integration, size of the integration domain, support domain for weight function, etc.

Errors in strain and stress evaluation can have several sources. Accuracy of the meshless methods is affected by several factors such as rounding errors in approximation or rounding errors caused by the numerical integration. The above mentioned errors become evident in differences between the reference and computed values. Both FEM softwares compute strain or stress values at the middle surface of the layer as the arithmetic mean of strain or stress values from top and bottom surface of the layer.

Acknowledgement

The authors gratefully acknowledge for support the Slovak and technology Assistance Agency registered under number APVV-0169-07, Slovak Grant Agency VEGA 1/1226/12.

References

Atluri, S. N. (2004): *The Meshless Method, (MLPG) For Domain & BIE Discretizations*, Tech Science Press.

Bensoussan, A.- Lion, J. L.- Papanicolaou, G. (1978) *Asymptotic analysis for periodic structures*. Amsterdam Holland.

Eshelby, J. D. (1957) The determination of elastic field of an ellipsoidal inclusion and related problems. in:*Proc. R. Soc. Londýn*, pp. 276- 396.

Hashin, Z.- Shtrikman, S. (1962) On some variational principles in anisotropic and nonhomogeneous elasticity, J. *Mech. Phys. Solids*, vol. 10, p.335-342.

Hill, R. (1965) A self-consistent mechanics of composite materials. In *J. Mech. Phys. Solids*, 13, pp. 213-222.

Christensen, R. M., Lo. K. H. (1979). Solutions for effective shear properties in three phase sphere and cylinder models, *J. Mech. Phys. Solids*, 27, pp. 315-330.

Mori, T.- Tanaka, K. (1973) Average stress in matrix and average elastic energy of materials with misfitting inclusion. *Acta Met.*, 21, pp. 571-574.

Norris, A. N. (1985) A differential scheme for the effective moduli of composites. *Mech. of Materials*, pp. 1-16.

Reddy J.N. (1997): *Mechanics of Laminated Composite Plates: Theory and Analysis*. CRC Press, Boca Raton.

Sladek, J., Sladek, V., Atluri, S. N. (2002) Application of the local boundary integral equation method to boundary-value problems. *Int. Appl. Mech*., 38, 9, pp. 1025- 1047.

Sladek, J.; Sladek, V.; Krivacek, J.; Wen, P.; Zhang, Ch. (2007): Meshless Local Petrov-Galerkin (MLPG) method for Reissner-Mindlin plates under dynamic load. *Computer Meth. Appl. Mech. Engn.*, 196: pp. 2681-2691.

Soares, D. Jr., Sladek, J., Sladek, V., Zmindak, M., Medvecky, S (2012): Porous Media Analysis by Modified MLPG Formulations. CMC: Computers, Materials,& Continua, 27,2, pp. 101-127.

Wallenberger, F. T., Bingham, P. A. (2010) Fiberglass and Glass Technology. Springer.